Available online at www.sciencedirect.com
SCIENCE DIRECT®
Biomaterials 26 (2005) 655–659
Biomaterials
www.elsevier.com/locate/biomaterials

Technical note

The potential of poly(*N*-isopropylacrylamide) (PNIPAM)-grafted hyaluronan and PNIPAM-grafted gelatin in the control of post-surgical tissue adhesions

Shoji Ohya[a,*], Hiromichi Sonoda[a,b], Yasuhide Nakayama[a], Takehisa Matsuda[b]

[a] *Department of Bioengineering, National Cardiovascular Center Research Institute, 5-7-1 Fujishirodai, Suita, Osaka 565-8565, Japan*
[b] *Division of Biomedical Engineering, Graduate School of Medicine, Kyushu University, 3-1-1 Maidashi, Higashi-ku, Fukuoka 812-8582, Japan*

Received 12 February 2004; accepted 13 March 2004

Abstract

Poly(*N*-isopropylacrylamide)-grafted hyaluronan (PNIPAM–HA) and PNIPAM-grafted gelatin (PNIPAM–gelatin), which exhibit sol-to-gel transformation at physiological temperature, were applied as control of tissue adhesions: tissue adhesion prevention material and hemostatic aid, respectively. The rat cecum, which was abraded using surgical gauze, was coated with PNIPAM–HA-containing PBS (concentration: 0.5 w/v%). The coated solution was immediately converted to an opaque precipitate at body temperature, which weakly adhered to and covered the injured rat cecum. One week after coating, tissue adhesion between the PNIPAM–HA-treated cecum and adjacent tissues was significantly reduced as compared with that between non-treated tissue and adjacent tissues. On the other hand, the coating of bleeding spots of a canine liver with PNIPAM–gelatin-containing PBS (concentration: 20 w/v%) resulted in spontaneous gel formation on the tissues and subsequently suppressed bleeding. Although these thermoresponsive tissue adhesion prevention and hemostatic materials are still prototypes at this time, both thermoresponsive biomacromolecules bioconjugated with PNIPAM, PNIPAM–HA and PNIPAM–gelatin, may serve as a tissue adhesion prevention material and hemostatic aid, respectively.

Keywords: Poly(*N*-isopropylacrylamide)-grafted biomacromolecules; Gel; Thermoresponsiveness; Tissue adhesion prevention; Hemostasis

1. Introduction

The prompt management of normal wound healing during and after surgical treatment may predict the post-surgical healing of tissues. Hemostatic control during surgical operation and tissue adhesion prevention after surgery are two critical issues in wound healing. To this end, various approaches and materials have been developed and tested over the years. However, "ideal" wound-healing materials have not been realized as yet.

Post-surgical tissue adhesion, which results from malignant healing response of a damaged tissue to a non-injured tissue, often causes life-threatening complications or necessitates re-operation. To reduce tissue adhesion, the use of physical barrier membranes to separate adjacent tissues during the healing process has been proposed and examined [1]. Carboxymethylcellulose [1,2], dextran [3] and oxidized regenerated cellulose [1–4] films have been clinically used as such membranes with some therapeutic effects. Hyaluronan (HA), which is an extracellular matrix component, is known to temporarily prevent tissue adhesion [5] when such a solution is coated on damaged tissue. However, HA is rapidly biodegraded by hyaluronidase and removed away from the injury sites [6].

On the other hand, tissue adhesive glue or hemostatic aids have been used when bleeding cannot be controlled during surgery. Fibrin glue has been clinically used in these cases. However, its major drawbacks are its low mechanical strength and potential infection risk inherent to blood origin. Semisynthetic and synthetic materials such as cyanoacrylate derivatives [7,8], gelatin–resorcinol–formaldehyde [8], and fluorinated hexamethylene diisocyanate-based urethane prepolymers [9] have been applied as surgical adhesives. Although they have

*Corresponding author. Tel.: +81-6-6833-5012; fax: +81-6-6872-8090.
E-mail address: ohya@ri.ncvc.go.jp (S. Ohya).

0142-9612/$ - see front matter © 2004 Elsevier Ltd. All rights reserved.
doi:10.1016/j.biomaterials.2004.03.002

appropriate tissue adhesiveness, cytotoxicity and severe inflammatory reactions with the use of the former two glues and very slow degradation with the last glue are the major drawbacks, respectively.

Regardless of tissue adhesion prevention or hemostatic aids, rapid sol-to-gel formation is necessary to cover the injured or bleeding sites of a tissue. Such a phase transition is desired to occur within a few minutes after application at physiological temperature. We previously prepared poly(*N*-isopropylacrylamide) (PNIPAM)-grafted hyaluronan (PNIPAM–HA) [10,11] and PNIPAM-grafted gelatin (PNIPAM–gelatin) [12–14]. These were soluble in water at room temperature but precipitated or gelled at physiological temperature due to thermoresponsive phase transition characteristics of PNIPAM. In this study, we explored the potential applicability of thermoresponsive PNIPAM–HA and PNIPAM–gelatin as a tissue adhesion prevention material or hemostatic aid, respectively.

2. Materials and methods

2.1. Material

Sodium hyaluronate (HANa, molecular weight: ca. 5.0×10^5 g/mol) was supplied by Seikagaku Kogyo Co. Ltd., Gelatin (molecular weight: ca. 9.5×10^4 g/mol, from bovine bone) and the solvents, which were of special reagent grade, were purchased from Wako Pure Chemical Industry Ltd., (Osaka, Japan) and used after conventional purification.

2.2. Cell adhesion on PNIPAM–HA film

An aqueous solution of PNIPAM–HA (concentration: 0.5 w/v%) was coated onto a circular cover glass (diameter: 14.5 mm, Matsunami Glass Co. Ltd., Osaka, Japan) and dried at room temperature. Rat fibroblasts at a density of 2.0×10^4 cells/ml were seeded on PNIPAM–HA films. After 3 h of incubation, cell morphology was observed by phase-contrast microscopy (Diaphoto, Nikon, Tokyo, Japan). All the procedures including cell culture were carried out at 37°C.

2.3. Tissue adhesion prevention efficacy of PNIPAM–HA

Tissue adhesion prevention efficacy was assessed using a rat cecum abrasion model [1,4]. Anesthesized Wistar rats were subjected to laparotomy. Each rat cecum was abraded with a surgical gauze. A PBS (0.5 ml) of PNIPAM–HA (concentration: 0.5 w/v%) was coated onto the cecum. One week after application, the incidence and severity of adhesions of the cecum to adjacent tissues were evaluated according to the following system: after harvesting the cecum and fixing it in formalin neutral buffer solution (pH 7.4, Wako Pure Chemical Industry Ltd., Osaka, Japan) at 37°C, the specimens stained with hematoxylin–eosin (H&E) and Masson's trichrome were observed by light microscopy (VANOX-S, Olympus, Tokyo, Japan).

0: No cecum adhesions
1: Firm adhesion with easily dissectable plane
2: Adhesion with dissectable plane causing mild tissue trauma
3: Fibrous adhesion with difficult tissue dissection
4: Fibrous adhesion with non-dissectable tissue planes.

2.4. Histological analysis of tissue adhesion prevention efficacy for PNIPAM–HA precipitate

For histological analysis, PNIPAM–HA-treated rat ceca, after seven days, were fixed with 10% formalin neutral buffer solution (pH 7.4) for more than seven days, dehydrated in a graded ethanol series, embedded in paraffin, and sectioned at 5 μm thickness. After staining with H&E or Masson's trichrome, the specimens were evaluated by light microscopy.

2.5. Hemostatic characteristics of PNIPAM–gelatin

The hemostatic characteristics of PNIPAM–gelatin were evaluated using a canine liver model (weight: 25 kg) and a Wistar rat aorta model (average weight: 250 g). The canine liver was abraded with trephine in laparotomy and the rat aorta was clamped and punctured using a 23-gage needle. A PBS of PNIPAM–gelatin (concentration: 20 w/v%) was coated on the bleeding spot. The efficacy of hemostasis was determined by gross observation.

3. Results

3.1. PNIPAM–HA

When rat fibroblasts were seeded and cultured on PNIPAM–HA film, cast from their aqueous solution, a markedly reduced adhesion and suppressed spreading (mostly round shape) were observed (Fig. 1), indicating that PNIPAM–HA is a non-cell-adhesive matrix.

The efficacy of the PNIPAM–HA film for tissue adhesion prevention was evaluated using a rat cecum abrasion model [1,4]. When a PBS solution of PNIPAM–HA was coated on a rat cecum, an opaque PNIPAM–HA precipitate was immediately formed around the cecum at body temperature. One week after coating, ceca without PNIPAM–HA coating strongly adhered to adjacent tissues (Figs. 2 and 3). When the adhesion incidence of each rat was scored according to the scoring

rate described in Section 2, the average overall score (4: severe adhesion, 0: non-adhesion) was 2.2 ± 0.7 ($n=9$) and the experimental sample number over score 2, which shows tissue adhesion, was counted as eight out of nine rats examined (Table 1). On the other hand, the reduced adhesion of the cecum to adjacent tissues was observed, although the PNIPAM–HA-treated ceca weakly adhered to adjacent tissues (Figs. 2 and 3). The average overall score was 1.3 ± 0.5 ($n=8$). The experimental sample number over score 2 was two out of eight rats examined (Fig. 2 and Table 1). These results indicate that the in situ formed PNIPAM–HA precipitate significantly reduced the degree of adhesion and occurrence of tissue adhesion of the rat cecum to adjacent tissues.

3.2. PNIPAM–gelatin

A PBS solution of PNIPAM–gelatin (20 w/v%) was coated on the bleeding spots generated by pricking a canine liver and a rat aorta with a needle. The solution was immediately converted to an elastic hydrogel on the

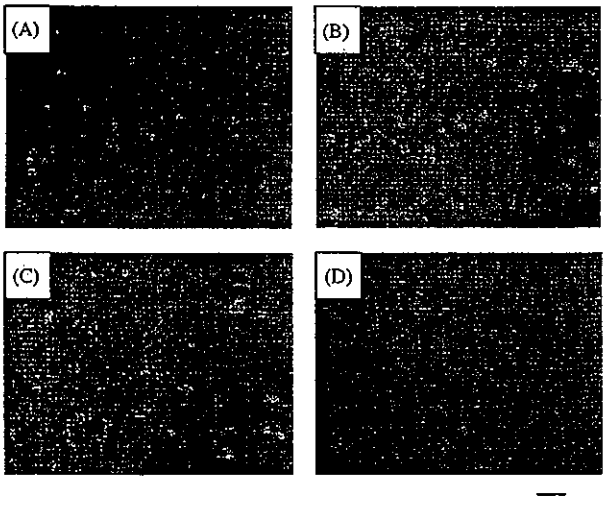

Fig. 1. Phase-contrast micrographs of rat fibroblasts (seeding density: 2.0×10^4 cells/ml) on glass (A)(C), PNIPAM–HA (B)(D) surfaces at 37°C immediately (A)(B) or after 3-h incubation (C)(D).

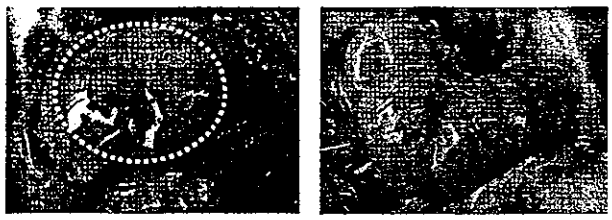

Fig. 2. Gross observation of PNIPAM–HA-treated cecum adhering to adjacent tissues one week after coating. Left: Non-PNIPAM–HA-treated cecum where omentum tissue adhered to and covered the injured cecum. Right: PNIPAM–HA-treated cecum without tissue adhesion.

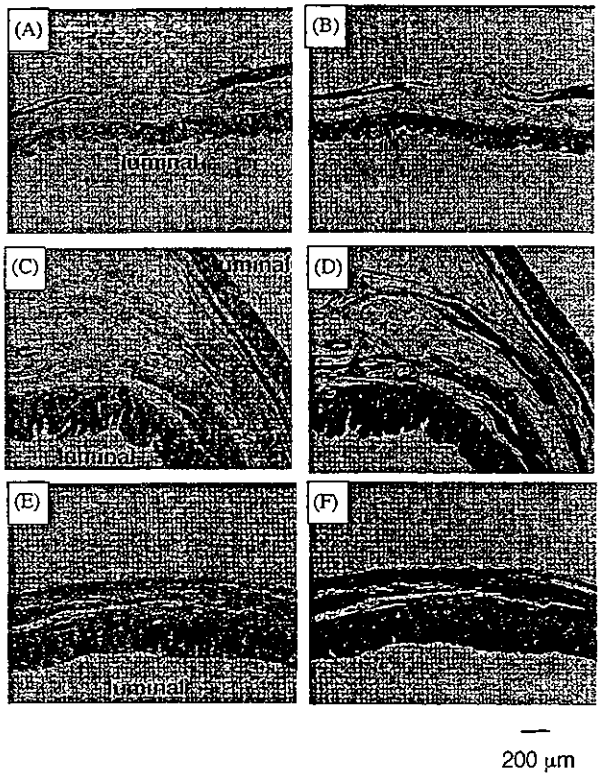

Fig. 3. Histological analysis of PNIPAM–HA-treated cecum adhering to adjacent tissues. Specimens were stained with H&E (A)(C)(E) and Masson's trichrome (B)(D)(F). PNIPAM–HA-treated cecum: (A) and (B), immediately after covering (E) and (F), 7 days after coating. Non-PNIPAM–HA-treated cecum: (C) and (D), 7 days after coating.

Table 1
Adhesion score of rat cecum

Sample	Adhesion score[a]	n	Ratio ⩾score 2
Non-treated	2.2 ± 0.7	9	8/9
PNIPAM-HA-treated	1.3 ± 0.5	8	2/8

[a] Adhesion scores are as follows: 0: No cecum adhesions, 1: Firmly adhesion with easily dissectable plane, 2: Adhesion with dissectable plane causing mild tissue trauma, 3: Fibrous adhesion with difficult tissue dissection, 4: Fibrous adhesion with nondissectable tissue planes.

bleeding spots (Fig. 4). The hydrogel weakly adhered to and covered the injured sites, resulting in hemostasis, which was completed within a minute after coating (Fig. 4). Pulsation was maintained, and no bleeding was observed within the experimental time observed (1–2 h after application).

4. Discussion

Fundamental requirements for "ideal" wound-healing materials are as follows: (1) viscous liquid form to

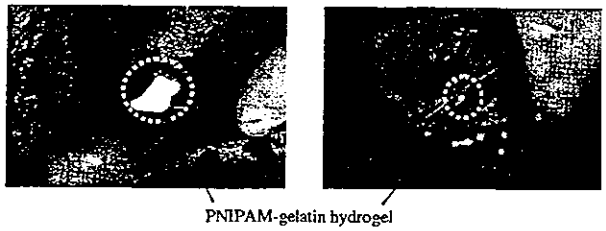

Fig. 4. Hemostases of bleeding from canine liver (left) and rat aorta (right) covered with PNIPAM–gelatin solution (20 w/v%). Spontaneous hydrogel formation and hemostases were observed. No rebleeding was observed during 1-h after coating. Pulsatile-induced periodic dilation/contraction was observed on the dissected rat aorta.

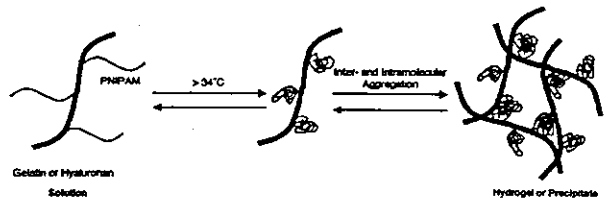

Fig. 5. Thermoresponsive gelation mechanism of PNIPAM–HA and PNIPAM–gelatin. Due to the dehydration of the hydrated amide group above lower critical solution temperature (LCST), PNIPAM graft chains were precipitated to form multimolecular aggregates. At high concentrations of PNIPAM-grafted biomacromolecules, the entire solution gelled to produce an opaque hydrogel and at low concentrations, a white precipitate was obtained.

completely cover complex-shaped tissue surfaces, (2) rapid formation of a swollen gel-like film or a precipitate when applied to injured tissues, (3) non-cell adhesiveness for tissue adhesion prevention and cell adhesiveness for hemostatic aids, and (4) appropriate biodegradability. That is, a wound-healing material should be biodegraded and sorpted with normal healing. Although various approaches and attempts have been carried out to meet the requirements listed above, in situ-applicable liquid-type materials, which include cyanoacrylate and fibrin glue, are limited (the major drawbacks associated with these hemostatic aids are described in Section 1) [7–9]. In this article, we applied thermoresponsive biomacromolecules (PNIPAM–HA and PNIPAM–gelatin) as wound-healing materials to meet the target requirements as listed above.

On a PNIPAM–HA film, cast from its aqueous solution at room temperature, the adhesion and spreading of fibroblasts were markedly inhibited (Fig. 1), which is due to the very highly swollen gel-like structure of HA (Fig. 5). When such a solution was applied to a rat cecum tissue, a slightly opaque precipitate was spontaneously formed. One week after application, markedly reduced adhesion of the PNIPAM–HA-treated cecum to adjacent tissues was observed while the non-treated cecum adhered to adjacent tissues, producing collagenous tissues (Fig. 3 and Table 1). Thus, in situ swollen precipitate of PNIPAM–HA effectively functioned in preventing tissue adhesion between the cecum and adjacent tissues.

As for thermoresponsive hemostatic aids, our previous study showed that PNIPAM–gelatin served as an artificial extracellular matrix material: the aqueous solution of PNIPAM–gelatin was immediately converted to a hydrogel, in which cells can adhere and proliferate. When PNIPAM–gelatin-containing PBS was coated on the bleeding sites of the canine liver and rat aorta, the solution was immediately converted to an opaque elastic hydrogel (Fig. 4). The hydrogel fully covered and weakly adhered to the bleeding sites, resulting in complete hemostasis on both tissues. The PNIPAM–gelatin-coated aorta pulsated well, indicating that the PNIPAM–gelatin formed quite elastic hydrogel and the hydrogel did not interfere with the periodic pulsation of a high-pressure circulatory system.

5. Conclusion

Although this article describes very limited experiments on tissue adhesion control using PNIPAM–HA and PNIPAM–gelatin, the bioconjugation of thermoresponsive synthetic materials and extracellular-matrix derived biomacromolecules, which thermally form precipitate or hydrogel, can provide a new prototype of wound-healing materials and promising procedures. Further studies to improve the properties required for both tissue adhesion and tissue adhesion prevention and to examine a longer term performances are needed. Such studies are ongoing in our laboratory.

Acknowledgements

The authors are grateful to Seikagaku Kogyo Co. Ltd., for the supply of sodium hyaluronate. This study was financially supported by Ministry of Education, Culture, Sports, Science and Technology under Grant No. 14780665 and No. 15200038.

References

[1] diZerega GS. Contemporary adhesion prevention. Feritl Steril 1994;61:219–35.
[2] Burns JW, Colt MJ, Burgess LS, Skinner KC. Preclinical evaluation of seprafilm™ bioresorbable membrane. Eur J Surg 1997;577(suppl.):40–8.
[3] Diamond MP, DeCherney AH, Linsky CB, Cunninghan T, Constantine B. Assesment of carboxymethylcellulose and 32% dextran 70 for prevention of adhesions in rabbit uterine horn model. Int J Fertil 1988;33:278–82.
[4] Linsky CB, Cohen SM, Franklin RR, Haney AF, Malinak LR, Patton GW, Rock JA, Rosenberg SM, Webster BW, Yuzpe AA. Prevention of postsurgical adhesions by INTERCEED(TC7), an

absorbable adhesion barrier: a prospective randomized multicenter clinical study. Feritil Steril 1989;51:933–8.
[5] Burns JW, Skinner K, Colt J, Sheidlin A, Bronson R, Yaacobi Y, Goldberg EP. Prevention of tissue injury and postsurgical adhesions by precoating tissues with hyaluronic acid solutions. J Surg Res 1995;59:644–52.
[6] Campoccia D, Doherty P, Radice M, Brun P, Abatangelo G, Williams DF. Semisynthetic resorbable materials from hyaluronan esterification. Biomaterials 1998;19:2101–27.
[7] Spotniz WD. History of tissue adhesives. In: Sierra D, Saits R, editors. Surgical adhesives and sealants, current technology and applications. USA: Technomic; 1996. p. 3–11.
[8] Tseng YC, Hyon SH, Ikada Y, Shimizu Y, Tamura K, Hitomi S. In vivo evaluation of 2-cyanoacrylates as surgical adhesives. J Appl Biomater 1990;1:111–9.
[9] Matsuda T, Nakajima N, Itoh T, Takakura T. Development of a compliant surgical adhesive derived from novel fluorinated hexamethylene diisocyanate. ASAIO 1989;35:381–3.
[10] Ohya S, Nakayama Y, Matsuda T. Thermoresponsive artificial extracellular matrix for tissue engineering: hyaluronic acid bioconjugated with poly(*N*-isopropylacrylamide) grafts. Biomacromolecules 2001;2:856–63.
[11] Ohya S, Nakayama Y, Matsuda T. Artificial extracellular matrix design in tissue engineering: synthesis of thermoresponsive hyaluronic acid and its supramolecular organization. Jpn J Artif Organs 2000;29:446–51.
[12] Morikawa N, Matsuda T. Thermoresponsive artificial extracellular matrix: *N*-isopropylacrylamide-graft-copolymerized gelatin. J Biomater Sci, Polym Ed 2002;13:167–83.
[13] Matsuda T. Molecular design of functional artificial extracellular matrix: thermoresponsive gelatin. Jpn J Artif Organs 1999;28:242–5.
[14] Ohya S, Nakayama Y, Matsuda T. Material design for artificial extracellular matrix: cell entrapment in poly(*N*-isopropylacrylamide) (PNIPAM)-grafted gelatin hydrogel. J Artif Organs 2001;4:308–14.

TISSUE ENGINEERING
Volume 10, Number 11/12, 2004

Novel Strategy for Soft Tissue Augmentation Based on Transplantation of Fragmented Omentum and Preadipocytes

TEIICHI MASUDA, M.D.,[1,2] MASUTAKA FURUE, M.D., Ph.D.,[2] and TAKEHISA MATSUDA, Ph.D.[1]

ABSTRACT

Current therapeutic procedures for soft tissue augmentation still lack the ability to induce rapidly formation of adipose tissue and its long-term stability, which is determined by rapid revascularization. The omentum is highly vascularized with microvascular endothelial cells (ECs) and is composed mainly of adipocytes that produce an enormously high level of vascular endothelial growth factor (VEGF). The aim of this study was to determine the potential usefulness of fragmented omentum tissues, with or without cotransplantation with preadipocytes, in soft tissue augmentation. Fragmented omentum tissues (approximately 500 mg) with or without preadipocytes (approximately 2.3×10^6) isolated from epididymal adipose tissues were transplanted under the dorsal skin of Wistar rats by percutaneous injection and the tissues were left under the skin for up to 12 weeks. Regardless of cotransplantation with preadipocytes, the general morphological features of the transplanted tissue were as follows. The transplanted tissues, the weight loss of which was limited to 30–40%, contained viable adipocytes and some pseudocysts surrounded by fibrotic septa with minor inflammatory cell infiltration. High levels of triacylglycerol content, capillary density, and VEGF production were observed in transplanted tissues 12 weeks postoperation. Cotransplantation with preadipocytes enhanced adipose tissue formation significantly. These observations strongly indicate that transplantation of fragmented omentum tissues or cotransplantation with preadipocytes may be a promising therapeutic procedure for soft tissue augmentation.

INTRODUCTION

DESPITE MANY YEARS OF EFFORT, various attempts, and clinical trials and practices, the reconstruction of soft tissue defects is still unsatisfactory in outcome and presents unsolved problems. Therapeutic procedures for soft tissue augmentation are classified into three approaches (each of which has inherent problems). One approach is the autologous transplantation of adipose tissues or adipocyte-rich tissues, which are harvested by suction or surgical excision.[1–8] The subcutaneous injection of suctioned adipose tissue, which gained popularity with the growing prevalence of liposuction techniques, resulted in continuous volumetric reduction with time, probably due to combined reasons such as the reduced viability of adipocytes as a result of suctioning, the low tolerance of adipocytes to ischemia, and the slow revascularization of transplanted tissue.[7,8] The second approach is the injection of a liquid synthetic polymer (silicone) or biomacromolecule-containing solution (collagen or hyaluronic acid).[9,10] The former has been abandoned because of toxicological problems and the latter has the shortcoming of fast volumetric loss due to rapid degradation and sorption. The latest approach is soft tissue augmen-

[1]Division of Biomedical Engineering, and [2]Department of Dermatology, Graduate School of Medical Sciences, Kyushu University, Fukuoka, Japan.

tation by tissue engineering: preadipocyte–polymer matrix constructs are inserted subcutaneously[11–16] or *in situ* adipose tissue formation is observed via the slow release of angiogenic factors or differentiating factors from implanted matrices.[16–20] The major shortcoming of this approach is retarded volumetric gain due to slow vascularization.

From the above-mentioned problems, it may be concluded that the requirements for soft tissue augmentation are (1) rapid volumetric gain to fill defects and (2) continuous maintenance of adipose tissue without time-dependent volumetric loss. It is strongly conceived that the rapid revascularization of transplanted adipose tissue is a crucial factor for the success of adipose tissue transplantation.

The omentum is a large plica of the mobile peritoneum, is highly vascularized, and is filled with adipose tissue.[21] In addition to the enormous number of microvascular endothelial cells (ECs)[22] in its tissue, the omentum has a high vascularization capacity,[23] which has been proven by the fact that the omentum is used as a pedicle graft for brain,[24] heart,[25] and lower extremity revascularization.[26] One study revealed that among various cell types in the body, adipocytes in the omentum are characterized by the highest production of vascular endothelial growth factor (VEGF), a major angiogenic factor.[27]

The omentum has been used for soft tissue augmentation of breasts and facial contour defects as a pedicle flap or a free flap, using microvascular anastomosis, and cosmetic results were reported satisfactory.[28–31] The usefulness of free omental grafts in soft tissue augmentation, however, has not been fully evaluated. Almost two decades ago, a preliminary report on the experimental study of free omental grafts (without fragmentation) showed that a considerable volumetric gain was achieved in the early phase of transplantation but ischemic necrosis at the central area of the transplanted tissue was noted.[32] No further study was reported despite promising results.

In this article, to overcome the problems mentioned above and to maximally utilize the inherent nature of omentum tissues, fragmented or minced omentum tissues were subcutaneously injected, and the time-dependent changes in tissue morphogenesis were examined: at the tissue, cellular, and genetic levels. The advantage of injection is that it enables the transplantation of tissue without major scarring, which is inevitable when tissue transplantation was performed by surgical procedures. Preadipocytes were expected to contribute to regenerate adipose tissue.

The results of this study were compared with those of the cotransplantation of fragmented omentum tissues with preadipocytes. The potential usefulness of fragmented omentum tissue in soft tissue augmentation in clinical settings is discussed.

MATERIALS AND METHODS

Materials

Collagenase (type II), dexamethasone, isobutyl methylxanthine (IBMX), and 3,3-diaminobenzidine were purchased from Sigma (St. Louis, MO). Anti-human von Willebrand factor (vWF) antibody, anti-rat proliferating cell nuclear antigen (PCNA) antibody, and peroxidase-conjugated IgG antibody were purchased from Dako-Cytomation (Carpinteria, CA). All other reagents were purchased from Wako Pure Chemical Industries (Osaka, Japan).

Isolation and culture of rat preadipocytes

Animal experiments were reviewed by the Committee of Ethics on Animal Experimentation of the Faculty of Medicine, Kyushu University (Fukuoka, Japan) and carried out in accordance with the *Guidelines for Animal Experiments* of the Faculty of Medicine, Kyushu University and the Law (No. 105) and Notification (No. 6) of the Japanese Government. Six-week-old male Wistar rats weighing 200 to 250 g (Kyudou, Saga, Japan) were anesthetized by intraperitoneal injection of pentobarbital sodium (40 mg/kg). Epididymal adipose tissues were aseptically harvested and placed in a 4°C saline solution supplemented with penicillin (500 U/mL) and streptomycin (500 μg/mL). The harvested tissues were enzymatically digested in Dulbecco's modified Eagle's medium (DMEM) supplemented with 0.05% (w/v) type II collagenase and 5% (w/v) bovine serum albumin for 30 min at 37°C on a shaker. The digested tissues were filtered through a 250-μm pore size sieve and then through a 100-μm pore size filter to separate undigested debris and capillary fragments from preadipocytes. The filtered cell suspension was centrifuged and the resulting pellet of preadipocytes was then plated at 10^4 cells/cm^2 onto plastic culture dishes in DMEM supplemented with 10% fetal bovine serum (FBS), penicillin (100 U/mL), and streptomycin (100 μg/mL). During cell expansion, the preadipocytes were subcultured before confluency because contact inhibition initiates adipocyte differentiation and stops preadipocyte proliferation. The cells were expanded two times and subjected to *in vivo* experiments. The differentiation of preadipocytes into adipocytes was accomplished by culturing confluent monolayers of cells in DMEM with 10% FBS, penicillin (100 U/mL), streptomycin (100 μg/mL), insulin (10 mg/mL), 1 mM dexamethasone, 0.5 mM IBMX, and 200 mM indomethacin for 72 h. The medium was then withdrawn and replaced with DMEM with 10% FBS, penicillin (100 U/mL), streptomycin (100 μg/mL), and insulin (5 mg/mL) and the cell culture was continued. On day 7, Sudan II staining of cultured cells was performed and the morphological assessment of differentiation was microscopically

quantified by counting cells containing visible lipid droplets.[33,34] For each sample, five different fields were examined and the percentage of lipid-containing cells was determined with an optical microscope (TE300, Nikon, Tokyo, Japan) at ×200 magnification.

In vivo *experiments*

Thirty Wistar rats weighing 330 to 380 g were used. Rats were distributed to two experimental groups.

Group I: In 15 rats, the greater omentum was removed through a midline incision. After the omentum was fragmented into 1-2-mm^3 sizes with a scalpel, the fragments were washed twice with physiological saline and were mixed with preadipocytes previously isolated and cultured from the same rat according to the methods described above. The mixture of omentum fragments and preadipocytes harvested from the same rat was injected between the rat's dorsal skin and the underlying muscle by percutaneous injection (18-gauge needle with 1-mL syringe). The mean weight of the injected omentum fragments was 524.5 ± 42.8 mg and the mean number of injected preadipocytes was $(2.3 \pm 1.4) \times 10^6$.

Group II: Another set of 15 rats received an injection of omentum fragments in between the dorsal skin and the underlying muscle by percutaneous injection. The mean weight of the injected omentum fragments was 501.2 ± 55.4 mg.

The rats were killed with an overdose of intraperitoneal pentobarbital sodium (200 mg/kg body weight) 2, 4, or 12 weeks postoperation (five rats for each group, for each transplantation period). The transplanted tissues were removed and weighed for comparison of their weight with that at the time of transplantation. After the sample was weighed, half of the sample was fixed in 10% formalin and then embedded in paraffin and sectioned for hematoxylin and eosin (H&E) staining, and further immunohistochemical studies. The residual half was divided in two pieces; one was used for triacylglycerol (TG) content measurement and the other was kept frozen (−80°C) for reverse transcription-polymerase chain reaction (RT-PCR) and enzyme immunoassay studies.

Immunohistochemical studies

Deparaffinized cross-sections (4 μm thick) were incubated with antibodies to human vWF (1:1600 dilution) and rat PCNA (1:200 dilution) at 4°C for 16 h. After further incubation with a peroxidase-conjugated secondary antibody, peroxidase activity was visualized with 3,3′-diaminobenzidine. The immunostained sections were counterstained with hematoxylin. Ten different fields were selected for determining the number of capillaries and PCNA-positive cells under an optical microscope (TE300, ×200 magnification; Nikon).

In situ *labeling of apoptotic cells*

Apoptotic cells were visualized by the terminal deoxynucleotidetransferase-mediated deoxyuridine triphosphate (dUTP) nick end-labeling (TUNEL) method, using a commercially available *in situ* apoptosis detection kit (Takara *in situ* apoptosis detection kit; Takara Bio, Shiga, Japan). The sections were counterstained with hematoxylin. Ten different fields were selected for determining the number of apoptotic cells under an optical microscope (×200 magnification).

Triacylglycerol content

The TG content of each sample was determined as described previously.[20] Briefly, total lipid was extracted with chloroform–methanol (1:2) and TG content was measured with a triglyceride E-test kit (Wako Pure Chemical Industries) according to the manufacturer's instructions.

Reverse transcription-polymerase chain reaction

Total RNA was obtained from approximately 50 mg of the harvested samples using ISOGEN (Nippon Gene, Tokyo, Japan) according to the manufacturer's instruction. With a commercially available kit (Ready-to-Go T-primed first-strand kit; Amersham Biosciences, Piscataway, NJ), 3.5 μg of total RNA was reverse transcribed to cDNA and amplified by PCR. The primers used for the detection of VEGF mRNA were 5′-CCGAATTCACCAAAGAAAGATAGAACAAAG (sense) and 5′-GGTGAGAGGTCTAGTTCCCGA (antisense).[35] The PCR was performed under the following conditions: denaturation at 98°C for 2 min followed by 5 cycles of 30 s at 98°C, 30 s at 48°C, and 30 s at 72°C (first step); 30 cycles of 30 s at 98°C, 30 s at 57°C, and 30 s at 72°C (second step). The samples were then treated at 72°C for 7 min. The primers used in the detection of basic fibroblast growth factor (bFGF) mRNA were 5′-GCCTTCCCACCCGGCCACTTCAAGG (sense) and 5′-GCACACACTCCCTTGATGGACACAA (antisense).[36] The thermal cycler conditions consisted of 2 min of denaturation at 96°C followed by 35 cycles of 30 s at 96°C, 30 s at 60°C, and 30 s at 72°C. The samples were then treated at 72°C for 7 min. The primers used for the detection of hepatocyte growth factor (HGF) mRNA were 5′-GGGGAATGAAATGCAGTCAG (sense) and 5′-CCTGTATCCATGGATGCTTC (antisense).[37] The thermal cycler conditions consisted of 2 min of denaturation at 96°C followed by 30 cycles of 30 s at 96°C, 30 s at 56°C, and 30 s at 72°C. The samples were then treated at 72°C for 7 min. The primers used for the detection of glyceraldehyde-3-phosphate dehydrogenase (GAPDH) mRNA as a

positive control were 5′-ACCACAGTCCATGCCATCAC (sense) and 5′-TCCACCACCCTGTTGCTGTA (antisense) (Toyobo, Osaka, Japan). The thermal cycler conditions consisted of 2 min of denaturation at 98°C followed by 30 cycles of 60 s at 98°C, 60 s at 56°C, and 60 s at 72°C. The samples were then treated at 72°C for 7 min. The RT-PCR products were analyzed by electrophoresis on 2% agarose gels. The sizes of the expected products were 311, 239, and 107 bp, depending on splicing form for the mRNA of VEGF ($VEGF_{188}$, 311 bp; $VEGF_{164}$, 239 bp; $VEGF_{120}$, 107 bp), 179 bp for mRNA of bFGF, 314 bp for mRNA of HGF, and 452 bp for mRNA of GAPDH.

Enzyme immunoassay

Total protein was obtained from approximately 50 mg of the harvested samples, using ISOGEN according to the manufacturer's instructions. To quantify the levels of VEGF, bFGF, and HGF in the tissue lysate, a commercially available enzyme immunoassay kit was used (VEGF [ACCUCYTE; CytImmune Sciences, College Park, MD]; bFGF [Quantikine; R&D Systems, Minneapolis, MN]; HGF [rat HGF EIA, Institute of Immunology, Tokyo, Japan]) according to the manufacturer's instructions. For value standardization, total protein concentration was measured with a commercially available protein assay kit (Bio-Rad protein assay; Bio-Rad Laboratories, Hercules, CA).

Statistical analysis

Experimental results were expressed as means ± standard deviation (SD). The data were subjected to statistical analysis, using analysis of variance (ANOVA). Statistical analysis was carried out by ANOVA with paired t test or Bonferroni/Dunn post hoc test; $p < 0.05$ was considered statistically significant. All statistical analyses were performed with StatView 5.0 (SAS Institute, Cary, NC).

RESULTS

Transplantation

Approximately 500 mg of fragmented omentum tissues or a mixture of fragmented tissues and preadipocyte-containing cells (approximately 2.3×10^6) was autologously transplanted under rat dorsal skin and adipose tissue morphogenesis was examined with transplantation time at the tissue, cellular, and mRNA levels. Group I received fragmented omentum tissues and preadipocyte-containing cells, and group II received only fragmented omentum tissues. The fragmented omentum tissues before transplantation were found to be composed of adipose tissues and a well-developed capillary network (Fig. 1A). As for preadipocytes, they were isolated from epididymal adipose tissues and cultured in medium containing differentiation agents (insulin, dexamethasone, isobutyl methylxanthine, and indomethacin). The intracellular accumulation of fat droplets was observed by Sudan II staining (Fig. 1B), indicating that some cells differentiated into adipocytes under the culture conditions mentioned above. Morphological assessment of differentiation revealed that 39.2 ± 11.2% ($n = 19$) of cultured cell contained lipid droplets, indicating that approximately 40% of the transplanted cells were preadipocytes.

Gross observation of the transplanted area showed that the mass of tissue at transplantation gradually decreased in size as transplantation proceeded, even at 12 weeks postoperation (Fig. 2). Table 1 lists the time-dependent changes in the weight of transplanted tissues harvested at 2, 4, and 12 weeks postoperation (each, $n = 5$). The

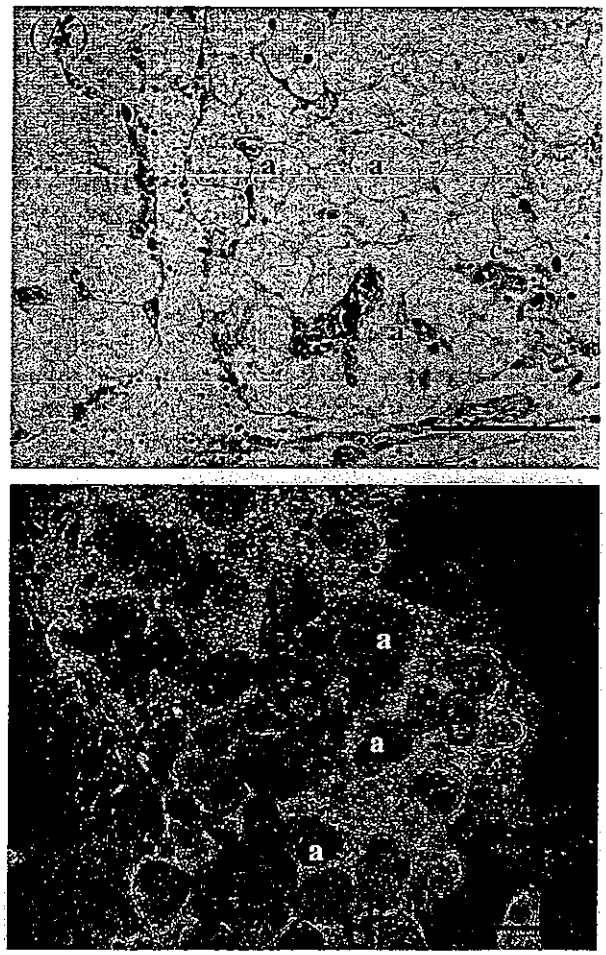

FIG. 1. (A) Omentum tissue (hematoxylin and eosin staining) composed of adipocytes (a) and well-developed capillary network (c). (B) Preadipocytes and differentiating adipocytes isolated from epididymal adipose tissue (Sudan II staining). Original magnification, ×200; scale bars, 100 μm.

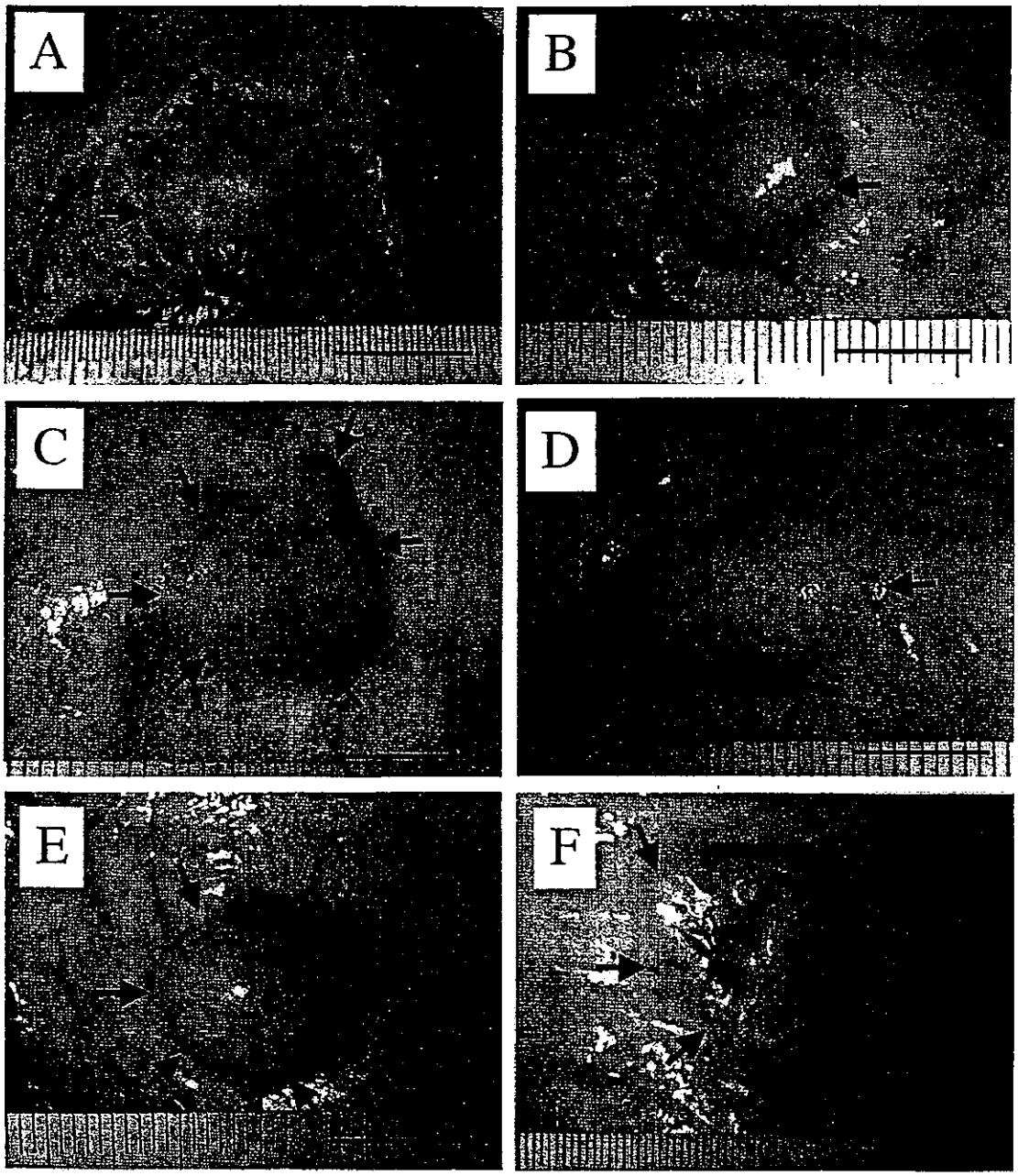

FIG. 2. Time-dependent changes in gross appearance of the transplanted area in group I [(A) 2 weeks postoperation; (B) 4 weeks postoperation; (C) 12 weeks postoperation] and group II [(D) 2 weeks postoperation; (E): 4 weeks postoperation; (F) 12 weeks postoperation]. Scale bars: 1 cm.

mean weights of harvested tissues were approximately 85% of the transplanted tissue at 2 weeks postoperation and 70% at 4 weeks postoperation, irrespective of the group. However, there were no significant time-dependent changes in the mean weights of transplanted tissues regardless of the group during these observation periods. At 12 weeks postoperation, the mean weights of tissues harvested decreased significantly to 60% of the transplanted tissues for group II ($p = 0.0072$), whereas there were no significant time-dependent changes in the mean weights of transplanted tissues in group I (mean, 71%).

Tissue morphology

Histological observations. Figures 3 and 4 show the H&E-stained sections of groups I and II at postoperative weeks 2 and 12. Irrespective of the group, the following general histological observations were made. At

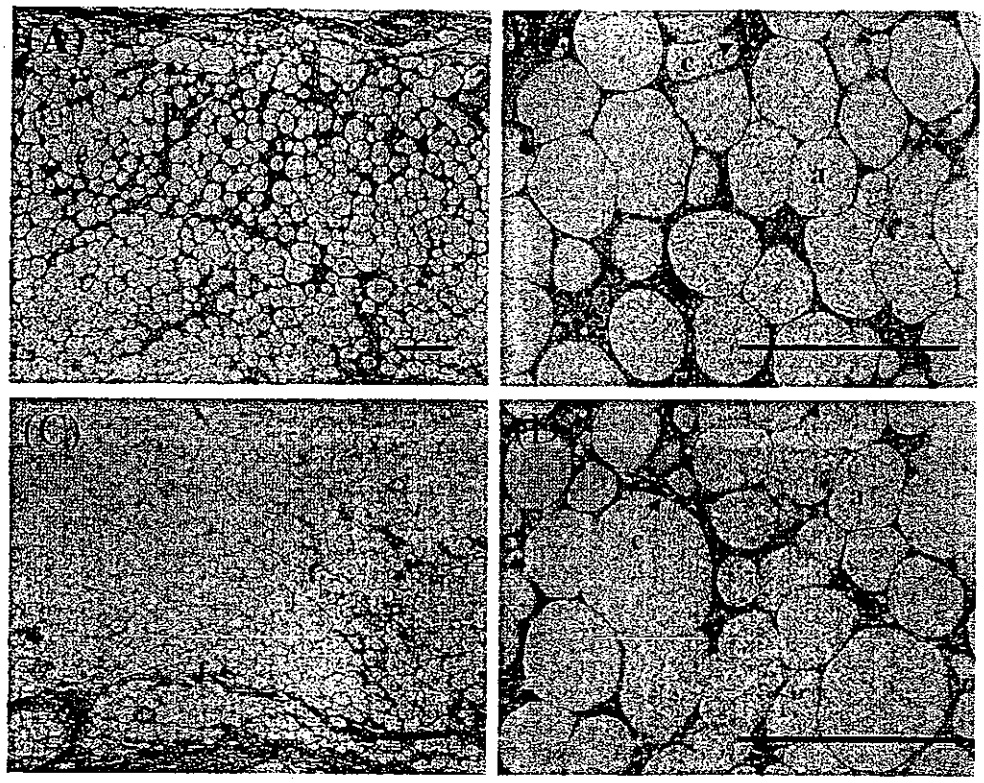

FIG. 3. Excised adiposed tissue after transplantation in group I [(A and B) 2 weeks postoperation; (C and D) 12 weeks postoperation]. a, adipocyte; c, capillary; f, fibrotic septa; p, pseudocyst. Hematoxylin and eosin staining. Original magnification: (A and C) ×40; (B and D) ×200. Scale bars: 200 μm.

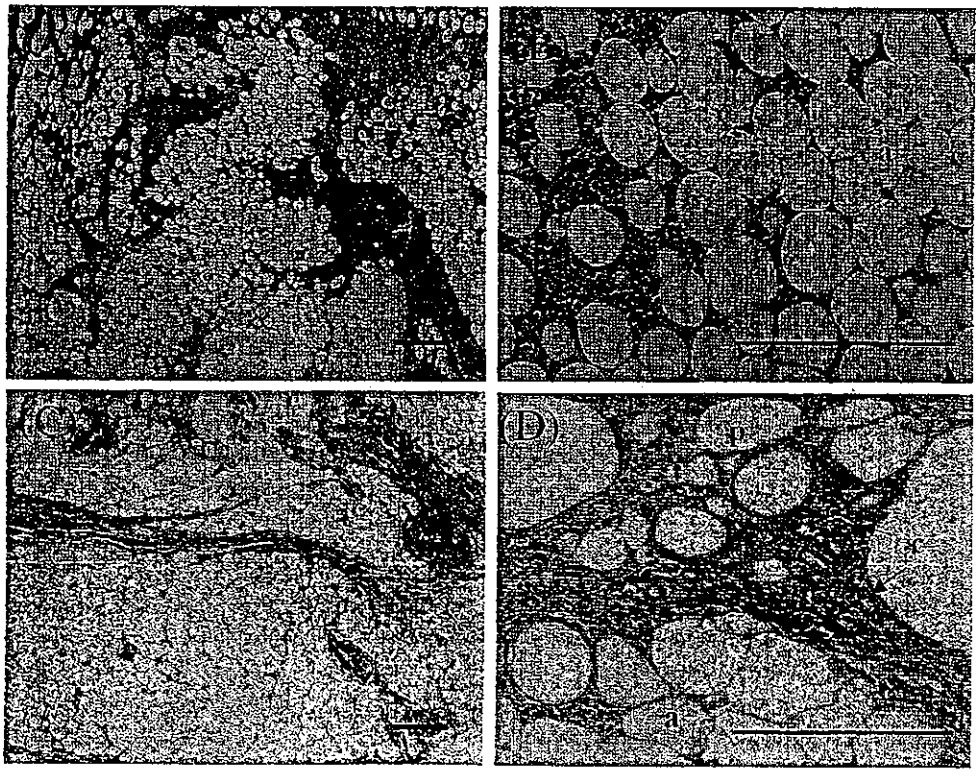

FIG. 4. Excised adiposed tissue after transplantation in group II [(A and B) 2 weeks postoperation; (C and D) 12 weeks postoperation]. a, adipocyte; c, capillary; f, fibrotic septa; p, pseudocyst. Hematoxylin and eosin staining. Original magnification: (A and C) ×40; (B and D) ×200. Scale bars: 200 μm.

2 weeks postoperation, an extensive infiltration of inflammatory cells into the viable fragmented omentum tissues was observed. The formation of pseudocysts, derived from the fusion of dead adipocytes, was observed around the area of cell infiltration (Fig. 3A and B and Fig. 4A and B). At 4 weeks postoperation, fibrosis became distinct between the viable fragmented omentum tissues and the infiltration of inflammatory cells around the viable adipocytes was markedly reduced (data not shown). At 12 weeks postoperation, the transplanted tissues were composed mainly of viable adipocytes and some pseudocysts surrounded by fibrotic septa with mild infiltration by inflammatory cells (Fig. 3C and D and Fig. 4C and D).

Capillary density. Immunohistochemical staining of von Willebrand factor (vWF) specific to endothelial cells was performed to determine the capillary densities of transplanted tissues. Capillary densities were found to be approximately 105 capillaries/mm^2 for omentum tissue, and 45 capillaries/mm^2 for the surrounding tissue to be transplanted. Capillary densities of transplanted tissues decreased significantly to approximately 60% of that of omentum tissue (approximately 65 capillaries/mm^2) at 2 weeks postoperation in groups I and II (group I, $p = 0.0006$; group II, $p = 0.0007$), but increased to the preoperation level at 4 weeks postoperative (Fig. 5). There was no significant difference in capillary density between groups I and II throughout the transplantation period. Capillary densities of the transplanted tissues in groups I and II were almost 1.5-fold to 2.5-fold higher than that of the surrounding tissue ($p = 0.001$–0.0066).

Proliferating and apoptotic cells. Immunohistochemical staining of proliferating cell antigen (PCNA) and the terminal deoxynucleotidetransferase-mediated deoxyuridine triphosphate (dUTP) nick end-labeling (TUNEL) method were used to determine the numbers of proliferating and apoptotic cells in transplanted tissues, respectively. The numbers of PCNA-positive cells were approximately 85 cells/mm^2 for the omentum tissue and 40 cells/mm^2 for the surrounding tissue to be transplanted. The numbers of TUNEL-positive cells were approximately 0.5 cell/mm^2 for the omentum tissue and 0.4 cell/mm^2 for the surrounding tissue to be transplanted. The numbers of PCNA-positive cells for the transplanted tissues at 2 and 4 weeks postoperation were almost 5-fold higher ($p = 0.0052$–0.0467) than for the omentum tissue or 10-fold higher ($p = 0.0052$–0.0252) than for the surrounding tissue (Fig. 6A). The numbers of TUNEL-positive cells for the transplanted tissues were almost 15-fold higher ($p = 0.0001$, group I; $p = 0.0003$, group II) at 2 weeks postoperation than for the omentum tissue in groups I and II (Fig. 6B). However, the numbers of PCNA-positive cells and apoptotic cells decreased considerably, approaching those of the surrounding tissues, at 12 weeks postoperation. There was no significant difference in the numbers of both PCNA- and TUNEL-positive cells between groups I and II throughout the transplantation period. Overall, the number of proliferating cells was almost 60- to 100-fold higher than that of apoptotic cells throughout the transplantation period.

Lipid accumulation

Triacylglycerol (TG) content, determined after extraction of total lipid from the transplanted tissues, was found to be approximately 560 mg/g for the omentum

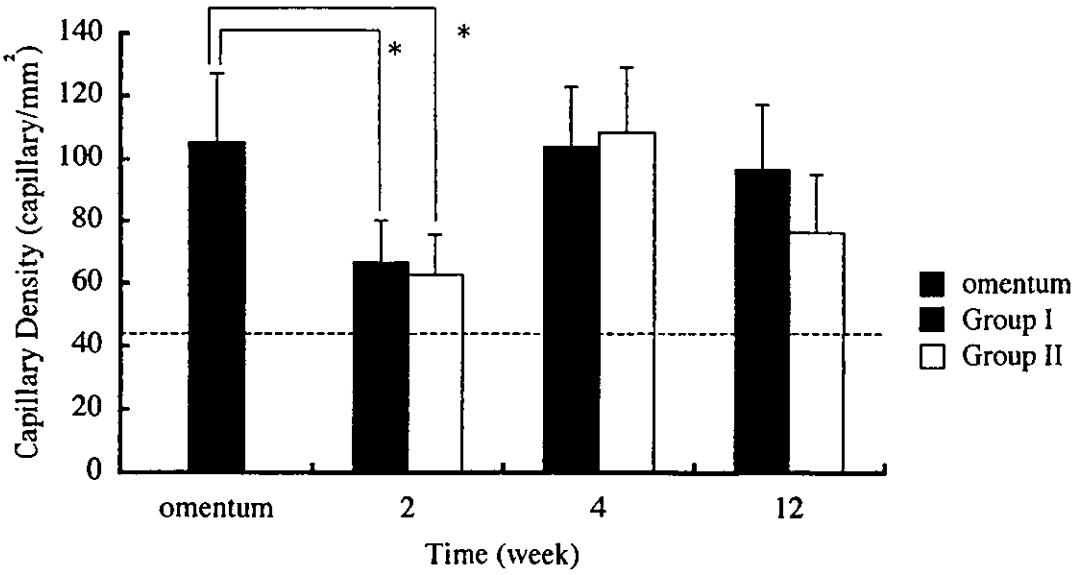

FIG. 5. Time-dependent changes in capillary densities of transplanted tissues (group I, solid columns; group II, open columns; each, $n = 5$). Dashed line indicates the capillary density of the surrounding subcutaneous tissue (42 capillaries/mm^2). Data represent means ± SD. $^*p < 0.05$.

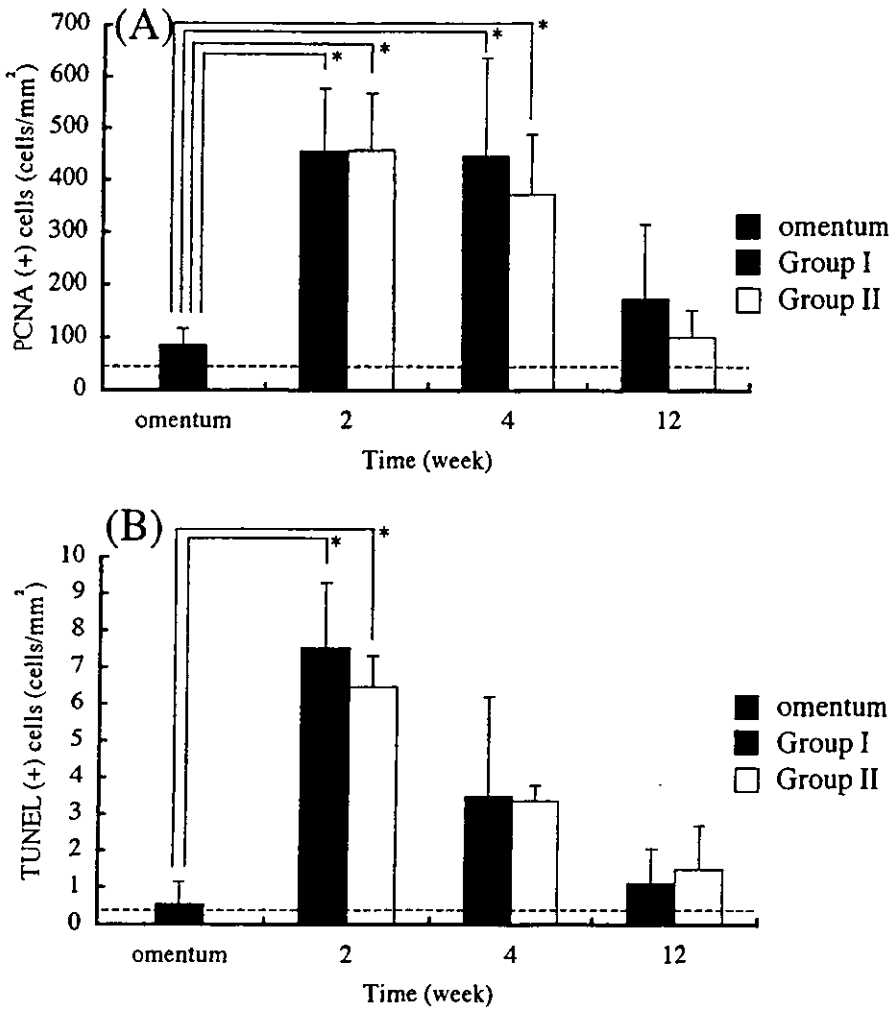

FIG. 6. Time-dependent changes in the numbers of PCNA-positive cells (**A**) and TUNEL-positive cells (**B**) of transplanted tissues (group I, solid columns; group II, open columns; each, $n = 5$). Dashed lines indicate the numbers of PCNA-positive cells (**A**, 42 cells/mm^2) and TUNEL-positive cells (**B**, 0.43 cell/mm^2) in the surrounding subcutaneous tissue. Data represent means ± SD. $*p < 0.05$.

tissue, and 17 mg/g for the surrounding tissue to be transplanted. In groups I and II, the TG content of transplanted tissues was almost one-half that of the omentum tissue at 2 and 4 weeks postoperation ($p = 0.0003$–0.0184). On the other hand, at 12 weeks postoperation, the TG content of transplanted tissues in group I increased to almost 75% of that of omentum tissue, but for group II it remained unchanged regardless of transplantation period (Fig. 7).

Growth factor expression and production

mRNA expression of three potent growth factors and angiogenic factors (HGF, bFGF, and VEGF) was determined by the RT-PCR technique. mRNA expression of HGF and bFGF was detected regardless of the transplantation period or group. As for VEGF, among the three isoforms, $VEGF_{164}$ (239 bp) and $VEGF_{120}$ (107 bp) had stronger mRNA signals and their continuous expression for both groups was observed throughout the transplantation period (Fig. 8).

The amount of VEGF, bFGF, and HGF produced in the transplanted tissues, determined by an enzyme immunoassay, showed that the amount of VEGF produced was approximately 4 ng/mg of protein in omentum tissue, and VEGF was not detected in the surrounding tissue to be transplanted. The amount of VEGF in the transplanted tissues produced ranged from 2.6 to 4.4 ng/mg of protein throughout the transplantation period (Fig. 9). There was no significant difference in terms of the amount of VEGF production throughout the transplantation period in groups I and II. bFGF and HGF protein was not detected (or was present at less than the detectable limit of enzyme immunoassay kits used) in the tissues regardless of the group or the transplantation period.

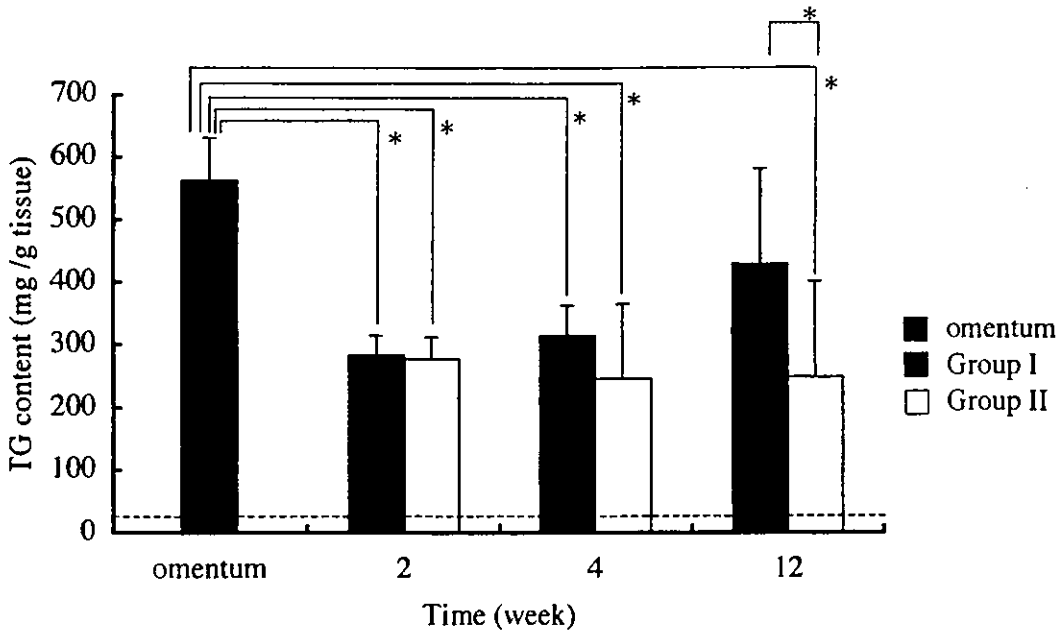

FIG. 7. Time-dependent changes in the triacylglycerol (TG) content of transplanted tissues (group I, solid columns; group II, open columns; each, $n = 5$). Dashed line indicates the triacylglycerol content of the surrounding subcutaneous tissue (17 mg/g tissue). Data represent means ± SD. $*p < 0.05$.

DISCUSSION

The major issue in soft tissue augmentation is the rapid generation of highly stable adipose tissues or adipose tissue substitutes with sufficient volume at the site of soft tissue defects. From this viewpoint, it still seems advantageous to transplant autologous adipocyte-rich tissues in clinical settings in spite of advances in adipose tissue engineering that enable the development of adipose tissues at a slow rate.

The omentum is highly vascularized with microvascular ECs[21,22] and is composed mainly of adipocytes that produce a high level of VEGF.[23,27] It is expected that a massive amount of supplied ECs and the potent angiogenic factor, VEGF, synergistically facilitate revascularization when fragmented omentum tissues are transplanted. In addition, the omentum exists in a relatively easily accessible intraabdominal structure, and its removal does not result in any functional deficit.[21] Few studies have been performed on the use of the omentum as a free graft for soft tissue augmentation. Das *et al.* reported a preliminary study in which rabbit free omentum was transplanted under the rabbit scalp and dorsal skin by surgical placement,[32] but no further study has been reported.

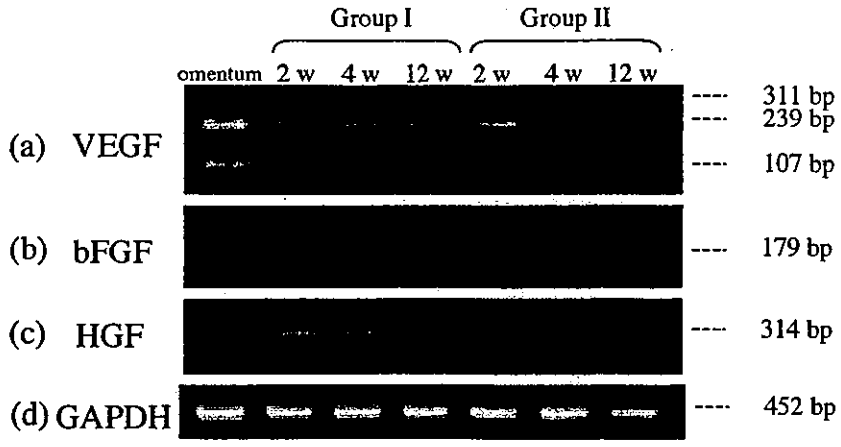

FIG. 8. Time-dependent changes in VEGF, bFGF, and HGF mRNA expression in transplanted tissues.

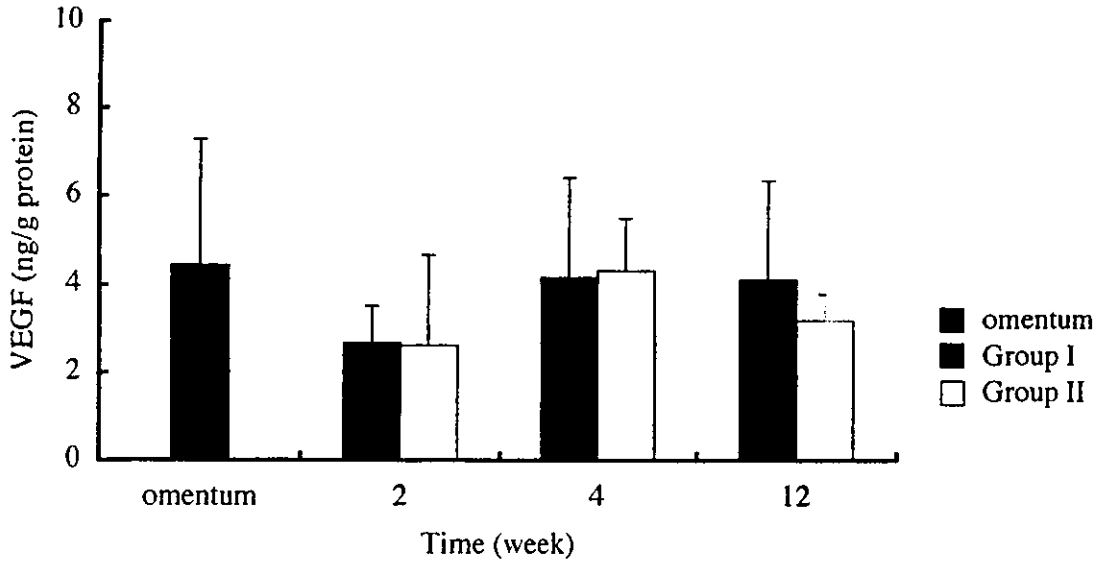

FIG. 9. Time-dependent changes in VEGF production in transplanted tissues (group I, solid columns; group II, open columns; each, $n = 5$). VEGF was not detected in the surrounding tissue to be transplanted.

This study was designed to determine the potential usefulness of the transplantation of fragmented omentum tissues or cotransplantation with preadipocytes in soft tissue augmentation. The transplanted tissues were evaluated in terms of gross appearance, weight change, tissue morphogenesis, and expression of angiogenic factors at the protein and genetic levels. The results are summarized as follows.

1. At 12 weeks postoperation, the transplanted tissue with minimal necrosis existed as a large mass (Fig. 2) and the weight losses of the transplanted tissues were limited to approximately 40% for group II (Table 1). Continuous weight losses among the transplanted tissues were noticed for group II (Table 1). On the other hand, although the initial loss of tissue in group I at the early transplantation period was noted to be similar to that in group II, such weight loss was not observed after 4 weeks of transplantation. There was a significant difference in weight loss between groups I and II at 12 weeks after transplantation. The reduced tissue loss observed for group I may be due to reduced necrosis and proliferation of preadipocytes and differentiation into mature adipocytes.

2. Extensive infiltration of inflammatory cells around the viable fragmented omentum tissues was observed at 2 weeks postoperation, followed by significant reduction in infiltration of inflammatory cells. The transplanted tissues were composed mainly of viable adipocytes and some pseudocysts surrounded by fibrotic septa at 12 weeks postoperation (Figs. 3 and 4).

3. The number of proliferating cells, which markedly exceeded that of apoptotic cells in the transplanted tissues, increased significantly during the early phase of transplantation (Fig. 6). It is presumed that the weight loss is due mainly to necrosis during the early phase of transplantation.

4. The TG content of the transplanted tissues was high compared with that of the surrounding tissue (almost 15-fold higher) for both groups I and II. These results sug-

TABLE 1. TIME-DEPENDENT CHANGES IN WEIGHT OF TRANSPLANTED TISSUES[a]

Group	Transplanted tissues (mg)	Transplanted cells ($\times 10^6$)	Transplantation period (week)[b]		
			2	4	12
I	524.5 ± 42.8	2.3 ± 1.4	85.9 ± 16.3	68.6 ± 21.8	71.1 ± 24.0
II	501.2 ± 55.4	—	84.5 ± 18.3	70.7 ± 15.8	59.9 ± 16.0[c]

[a]Weight percent relative to the initially transplanted tissues.
[b]$n = 5$ for each group and transplantation period.
[c]$p < 0.05$.

gest that addition of preadipocytes enhances the TG content of adipose constructs, which is probably due to differentiation of the transplanted preadipocytes into mature adipocytes (Fig. 7).

5. The capillary density of the transplanted tissues (approximately 65 capillaries/mm^2) decreased significantly to approximately 60% of that of omentum tissue at 2 weeks postoperation in groups I and II, but increased to the level of omentum tissue at 4 weeks postoperation (Fig. 5). The initial decrease in capillary density may be due to the acute necrosis of fragmented omentum tissues that failed to revascularize as the transplanted cells underwent more passive cellular necrosis rather than death by an active apoptotic process (Fig. 6).

6. VEGF mRNA expression and high VEGF production were observed throughout the transplantation period. HGF protein and bFGF protein were not detected, although the mRNAs for both growth factors were detected throughout the transplantation period (Figs. 8 and 9). These findings suggest that VEGF is the major factor contributing to the revascularization and angiogenesis of the transplanted tissues.

From this study it appears that the transplanted fragmented omentum tissues can survive as a free graft at least during the subacute phase (3 months) after transplantation. With this method, acute volumetric gains were noted right after transplantation and were maintained throughout the transplantation period; such gains cannot be obtained by previously reported methods of soft tissue augmentation based on tissue engineering. In addition, fragmented omentum tissues cotransplanted with preadipocytes have a better chance of forming a volumetric mass with a high triacylglycerol content. The advantage of using omentum tissue for soft tissue augmentation is that transplanted omentum tissues produce VEGF continuously after transplantation, which is greatly beneficial for revascularization and angiogenesis of the transplanted tissues. Das *et al.* reported that the mean survival of omentum grafts (not fragmented) at 3 months was 80 to 88%, as expressed in terms of weights of the surviving omentum compared with initial graft weight. However, they also reported that some amount of central necrosis was observed in the graft. Our results showed that there was no obvious central necrosis, indicating that fragmented omentum had a better chance of rapid revascularization for tissue survival compared with nonfragmented omentum tissue. This rapid revascularization and angiogenesis potential of fragmented omentum tissue also seem to play a substantial role in the survival and differentiation of preadipocytes when they are cotransplanted with omentum tissues. A major drawback of using omentum tissue is that a laparotomy is inevitable for harvesting the tissue. However, advances in laparoscopic surgery have enabled the harvesting of ometum with minimal invasion.[30,38] It is envisaged that optimization of the amount of fragmented omentum tissue and preadipocytes for transplantation and minimally invasive endoscopic harvesting of omentum tissues[38,39] may enable the realization of soft tissue augmentation in clinical settings; however, further longer term study, focusing on how to maintain the volumetric mass of fragmented omentum tissue–preadipocyte mixtures, must be done before clinical application.

ACKNOWLEDGMENT

This study was financially supported in part by a Grant-in-Aid for Scientific Research (A2-15200038) from the MEXT of Japan.

REFERENCES

1. Billings, E., Jr., and May, J.W., Jr. Historical review and present status of free fat graft autotransplantation in plastic and reconstructive surgery. Plast. Reconstr. Surg. **83,** 368, 1989.
2. Kononas, T.C., Bucky, L.P., Hurley, C., and May, J.W., Jr. The fate of suctioned and surgically removed fat after reimplantation for soft-tissue augmentation: A volumetric and histologic study in the rabbit. Plast. Reconstr. Surg. **91,** 763, 1993.
3. Fagrell, D., Enestrom, S., Berggren, A., and Kniola, B. Fat cylinder transplantation: An experimental comparative study of three different kinds of fat transplants. Plast. Reconstr. Surg. **98,** 90, 1996.
4. Nishimura, T., Hashimoto, H., Nakanishi, I., and Furukawa, M. Microvascular angiogenesis and apoptosis in the survival of free fat grafts. Laryngoscope **110,** 1333, 2000.
5. Chajchir, A. Fat injection: Long-term follow-up. Aesthetic Plast. Surg. **20,** 291, 1996.
6. Smahel, J. Experimental implantation of adipose tissue fragments. Br. J. Plast. Surg. **42,** 207, 1989.
7. Nguyen, A., Pasyk, K.A., Bouvier, T.N., Hassett, C.A., and Argenta, L.C. Comparative study of survival of autologous adipose tissue taken and transplanted by different techniques. Plast. Reconstr. Surg. **85,** 378, 1990.
8. Boschert, M.T., Beckert, B.W., Puckett, C.L., and Concannon, M.J. Analysis of lipocyte viability after liposuction. Plast. Reconstr. Surg. **109,** 761, 2002.
9. Robinson, J.K., and Hanke, C. W. Injectable collagen implant: Histopathologic identification and longevity of correction. J. Dermatol. Surg. Oncol. **11,** 124, 1985.
10. Elson, M. L. Soft tissue augmentation. Dermatol. Surg. **21,** 491, 1995.
11. Green, H., and Kehinde, O. Formation of normally differentiated subcutaneous fat pads by an established preadipose cell line. J. Cell. Physiol. **101,** 169, 1979.
12. Patrick, C.W., Jr., Chauvin, P.B., Hobley, J., and Reece, G.P. Preadipocyte seeded PLGA scaffolds for adipose tissue engineering. Tissue Eng. **5,** 139, 1999.

13. Schoeller, T., Lille, S., Wechselberger, G., Otto, A., Mowlawi, A., and Piza-Katzer, H. Histomorphologic and volumetric analysis of implanted autologous preadipocyte cultures suspended in fibrin glue: A potential new source for tissue augmentation. Aesthetic Plast. Surg. **25,** 57, 2001.
14. von Heimburg, D., Zachariah, S., Heschel, I., *et al.* Human preadipocytes seeded on freeze-dried collagen scaffolds investigated *in vitro* and *in vivo*. Biomaterials **22,** 429, 2001.
15. Halberstadt, C., Austin, C., Rowley, J., *et al.* A hydrogel material for plastic and reconstructive applications injected into the subcutaneous space of a sheep. Tissue Eng. **8,** 309, 2002.
16. Katz, A.J., Llull, R., Hedrick, M.H., and Futrell, J.W. Emerging approaches to the tissue engineering of fat. Clin. Plast. Surg. **26,** 587, 1999.
17. Kawaguchi, N., Toriyama, K., Nicodemou-Lena, E., Inou, K., Torii, S., and Kitagawa, Y. *De novo* adipogenesis in mice at the site of injection of basement membrane and basic fibroblast growth factor. Proc. Natl. Acad. Sci. U.S.A. **95,** 1062, 1998.
18. Tabata, Y., Miyao, M., Inamoto, T., *et al. De novo* formation of adipose tissue by controlled release of basic fibroblast growth factor. Tissue Eng. **6,** 279, 2000.
19. Yuksel, E., Weinfeld, A.B., Cleek, R., *et al. De novo* adipose tissue generation through long-term, local delivery of insulin and insulin-like growth factor-1 by PLGA/PEG microspheres in an *in vivo* rat model: A novel concept and capability. Plast. Reconstr. Surg. **105,** 1721, 2000.
20. Masuda, T., Furue, M., and Matsuda, T. Photocured-styrenated-gelatin microspheres for *de novo* adipogenesis through co-release of basic fibroblast growth factor, insulin, and insulin-like growth factor-1. Tissue Eng. **10,** 523, 2004.
21. Liebermann-Meffert, D. The greater omentum: Anatomy, embryology, and surgical applications. Surg. Clin. North Am. **80,** 275, 2000.
22. Chung-Welch, N., Patton, W.F., Shepro, D., and Cambria, R.P. Human omental microvascular endothelial and mesothelial cells: Characterization of two distinct mesodermally derived epithelial cells. Microvasc. Res. **54,** 108, 1997.
23. Goldsmith, H.S., Griffith, A.L., Kupferman, A., and Catsimpoolas, N. Lipid angiogenic factor from omentum. JAMA **252,** 2034, 1984.
24. Goldsmith, H.S., and Sax, D.S. Omental transposition for cerebral infarction: A 13-year follow-up study. Surg. Neurol. **51,** 342, 1999.
25. Vineberg, A. The bloodless greater omentum for myocardial revascularization. Dis. Chest **54,** 315, 1968.
26. Casten, D.F., and Alday, E.S. Omental transfer for revascularization of the extremities. Surg. Gynecol. Obstet. **132,** 301, 1971.
27. Zhang, Q.X., Magovern, C.J., Mack, C.A., Budenbender, K.T., Ko, W., and Rosengart, T.K. Vascular endothelial growth factor is the major angiogenic factor in omentum: Mechanism of the omentum-mediated angiogenesis. J. Surg. Res. **67,** 147, 1997.
28. McColl, I Reconstruction of the breast with omentum after subcutaneous mastectomy. Lancet **8108,** 134, 1979.
29. Walkinshaw, M., Caffee, H.H., and Wolfe, S.A. Vascularized omentum for facial contour restoration. Ann. Plast. Surg. **10,** 292, 1983.
30. Cothier-Savey, I., Tamtawi, B., Dohnt, F., Raulo, Y., and Baruch, J. Immediate breast reconstruction using a laparoscopically harvested omental flap. Plast. Reconstr. Surg. **107,** 1156, 2001.
31. Losken, A., Carlson, G.W., Culbertson, J.H., Hultman, C.S., Kumar, A.V., Jones, G.E., Bostwick, J., III, and Jurkiewicz, M.J. Omental free flap reconstruction in complex head and neck deformities. Head Neck **24,** 326, 2002.
32. Das, S.K., Cragun, J.R., Wheeler, E.S., Goshgarian, G., and Miller, T.A. Free grafting of the omentum for soft-tissue augmentation: A preliminary laboratory study. Plast. Reconstr. Surg. **68,** 556, 1981.
33. Gregoire, F., Genart, C., Hauser, N., and Remacle, C. Glucocorticoids induce a drastic inhibition of proliferation and stimulate differentiation of adult rat fat cell precursors. Exp. Cell Res. **196,** 270, 1991.
34. Hutley, L.J., Herington, A.C., Shurety, W., Cheung, C., Vesey, D.A., Cameron, D.P., and Prins, J.B. Human adipose tissue endothelial cells promote preadipocyte proliferation. Am. J. Physiol. Endocrinol. Metab. **281,** E1037, 2001.
35. Inoue, K., Sakurada, Y., Murakami, M., Shirota, M., and Shirota, K. Detection of gene expression of vascular endothelial growth factor and Flk-1 in the renal glomeruli of the normal rat kidney using the laser microdissection system. Virchows Arch. **442,** 159, 2003.
36. Casson, R.J., Wood, J.P., Melena, J., Chidlow, G., and Osborne, N.N. The effect of ischemic preconditioning on light-induced photoreceptor injury. Invest. Ophthalmol. Vis. Sci. **44,** 1348, 2003.
37. Shimazaki, K., Yoshida, K., Hirose, Y., Ishimori, H., Katayama, M., and Kawase, T. Cytokines regulate c-Met expression in cultured astrocytes. Brain Res. **962,** 105, 2003.
38. Saltz, R., Stowers, R., Smith, M., and Gadacz, T.R. Laparoscopically harvested omental free flap to cover a large soft tissue defect. Ann. Surg. **217,** 542, 1993.
39. Faga, A., Valdatta, L., Mezzetti, M., Buoro, M., and Thione, A. Ultrasound-assisted lipolysis of the omentum in dwarf pigs. Aesthetic Plast. Surg. **26,** 193, 2002.

Address reprint request to:
Takehisa Matsuda, Ph.D.
Department of Biomedical Engineering
Graduate School of Medical Sciences
Kyushu University
3-1-1 Maidashi, Higashiku
Fukuoka 812-8582, Japan

E-mail: matsuda@med.kyushu-u.ac.jp

UltraRapid Communication

Application of Nanoparticle Technology for the Prevention of Restenosis After Balloon Injury in Rats

Toyokazu Uwatoku, Hiroaki Shimokawa, Kohtaro Abe, Yasuharu Matsumoto, Tsuyoshi Hattori, Keiji Oi, Takehisa Matsuda, Kazunori Kataoka, Akira Takeshita

Abstract—Restenosis after percutaneous coronary intervention continues to be a serious problem in clinical cardiology. Recent advances in nanoparticle technology have enabled us to deliver an antiproliferative drug selectively to the balloon-injured artery for a longer time. NK911, which is a core-shell nanoparticle of polyethyleneglycol-based block copolymer encapsulating doxorubicin, accumulates in vascular lesions with increased permeability. We first confirmed that balloon injury caused a marked and sustained increase in vascular permeability (as evaluated by Evans blue staining) for a week in the rat carotid artery. We then observed that intravenous administration of just 3 times of NK911, but not doxorubicin alone, significantly inhibited the neointimal formation of the rat carotid artery at 4 weeks after the injury in both a single- and double-injury model. Immunostaining demonstrated that the effect of NK911 was due to inhibition of vascular smooth muscle proliferation but not to enhancement of apoptosis or inhibition of inflammatory cell recruitment. Measurement of vascular concentrations of doxorubicin confirmed the effective delivery of the agent to the balloon-injured artery by NK911 in both a single- and double-injury model. RNA protection assay demonstrated that NK911 inhibited expression of several cytokines but not that of apoptosis-related molecules. NK911 was well tolerated without any adverse systemic effects. These results suggest that nanoparticle technology to target vascular lesions with increased permeability is a promising and safe approach for the prevention of restenosis after balloon injury. The full text of this article is available at http://www.circresaha.org. (*Circ Res.* 2003;92:e62-e69.)

Key Words: nanoparticle ■ restenosis ■ angioplasty ■ drug delivery

Percutaneous transluminal coronary intervention (PCI) is now widely used for the treatment of coronary artery disease; however, restenosis after the procedure continues to be a serious complication.[1,2] Restenosis can be prevented by a local delivery of an antiproliferative agent to the dilated segment of the coronary artery. This strategy has been utilized for the treatment of cancers, and indeed many drug delivery systems (DDS) have been developed and tested for selective and efficient delivery of antiproliferative agents to tumor tissues.[3–13] Tumor tissues are characterized by enhanced permeability and retention (EPR) effects, which include hypervascularity, enhanced permeability, and low wash-out of a drug delivered to the tissue.[14] Recent advances in nanoparticle technology have enabled us to develop a nanoparticle carrier conjugated with an antiproliferative agent for the treatment of tumors with EPR effects. This includes NK911, which is a core-shell nanoparticle formed through a self-assembly of block copolymer conjugated with doxorubicin.[13] NK911 consists of shell-forming hydrophilic segment (polyethylene glycol) and doxorubicin-conjugated hydrophobic segment of polyaspartic acid. When NK911 is dissolved in the aqueous phase, it forms stable core-shell nanoparticles (polymeric micelles) with an average diameter of 40 nm and physically entraps free-doxorubicin to inner core (active component of the antiproliferative effect of NK911).[13] NK911 can selectively penetrate through a tumor-vessel wall with EPR effects.[13] Based on the previous reports concerning prolonged endothelial dysfunction after balloon injury,[15,16] we hypothesized that balloon-injured coronary arteries also have EPR effects, and thus could be a good target for NK911. This prompted us to examine whether NK911 is effective for the prevention of restenosis after balloon injury in the rat carotid artery.

Materials and Methods

This experiment was approved by the Institutional Animal Care and Use Committee and was conducted in conformity with institutional guidelines. NK911 was provided by Nippon Kayaku Pharmaceutical Co (Tokyo, Japan). The pharmacologically effective dose of doxorubicin released from NK911 is 16% of the micelle.[17]

Original received January 3, 2003; revision received March 14, 2003; accepted March 18, 2003.

From the Departments of Cardiovascular Medicine (T.U., H.S., K.A., Y.M., T.H., K.O., A.T.) and Biomedical Engineering (T.M.), Kyushu University Graduate School of Medical Sciences, Fukuoka, Japan; and the Department of Materials Science and Engineering (K.K.), Graduate School of Engineering, The University of Tokyo, Japan.

Correspondence to Hiroaki Shimokawa, MD, PhD, Department of Cardiovascular Medicine, Kyushu University Graduate, School of Medical Sciences, 3-1-1 Maidashi, Higashi-ku, Fukuoka 812-8582, Japan. E-mail shimo@cardiol.med.kyushu-u.ac.jp

Circulation Research is available at http://www.circresaha.org

DOI: 10.1161/01.RES.0000069021.56380.E2

Time Course of the Increase in Vascular Permeability After Balloon Injury

A single balloon injury was created with a Fogarty catheter in the normal left rat carotid artery as previously described.[18] Time course of the increase in vascular permeability was examined before, immediately after, and 1, 3, 5, and 7 days after the balloon injury (3 animals for each time point), when we administered Evans-Blue dye (35 mg/kg) intravenously and euthanized the animals 45 minutes after the administration. The balloon-injured carotid artery was carefully isolated, opened longitudinally, and analyzed at a magnification of 20×.

Single-Injury Model

Male Wistar-Kyoto rats (240 to 260 g) were anesthetized with intraperitoneal sodium pentobarbital (50 mg/kg), and then a balloon injury of the left carotid artery was made as previously described.[18] Six sham-operated rats also underwent the same surgical procedure except that the balloon was not inserted. NK911 (0.1, 1, and 10 mg/kg), doxorubicin alone (0.016, 0.16, and 1.6 mg/kg; adjusted for the corresponding content of doxorubicin in NK911) or saline vehicle was administered intravenously 3 times, immediately after, and 3 and 6 days after the balloon injury. For each dose, 6 animals were assigned in a random and blind manner. At 4 weeks after the balloon injury, the animals were killed with an overdose of pentobarbital, and the carotid artery was perfusion-fixed at 100 mm Hg with 10% formaldehyde, excised, and embedded in paraffin. The carotid segment (10 mm in length) was isolated from the middle of the balloon-injured artery, cut into 3 sections, and stained with hematoxylin-eosin in each rat (n=6 each for 3 doses of NK911 or doxorubicin alone). The medial and intimal areas, luminal area, and the length of the internal (IEL) and the external elastic lamina (EEL) were measured with a computerized digital image analysis system and averaged for 3 (distal, middle, and proximal) sections.

Double-Injury Model

In order to induce preceding vascular lesions, we made an initial balloon injury with a Fogarty catheter 2 weeks before creating a second balloon injury in the rat carotid artery. For the initial injury, we inserted the balloon catheter through the right iliac artery into the left carotid artery and performed balloon-injury of the artery as in the single-injury model. For the second injury, we inserted the catheter into the previously balloon-injured carotid artery, confirmed the position of the catheter under direct view, and performed balloon injury at the same site as in the first injury. The manner of drug administration (1 and 10 mg/kg for NK911 and 0.16 and 1.6 mg/kg for doxorubicin alone) and that of tissue analysis were the same as in the single-injury model. For each dose, 6 animals were assigned in a blind manner.

Cell Proliferation, Apoptosis, and Infiltration of Inflammatory Cells in the Injured Artery

In each serial section, proliferating cells were evaluated by PCNA staining and apoptotic cells by terminal deoxynucleotidyl transferase (TdT)–mediated dUTP nick end-labeling (TUNEL) method using an in vivo apoptosis detection kit (WAKO). Inflammatory cells were evaluated by ED-1 immunostaining. Those analyses were performed 7 days after the balloon injury based on the previous studies with the same rat model of balloon injury.[19,20] Six animals were assigned for 3 different doses of either NK911 or doxorubicin alone. In each experiment, rat small intestine was used as a positive control. A negative control was made without the PCNA, TdT, or ED-1 antibody. The number of cells positive for PCNA, TUNEL, or ED-1 staining was counted at a magnification of 400× in a blind manner. The quantitative analysis was performed in 3 sections (distal, middle, and proximal) from each carotid artery and averaged in each animal. The number of PCNA-positive cells in the 3 vascular layers (the intima, media, and adventitia) was counted for each section. The number of TUNEL-positive cells was expressed as a TUNEL index (TUNEL-positive cells/total nucleated cells). The number of ED-1–positive cells was counted in a whole section. All specimens were prepared at 1 week after the balloon injury.

RNA Protection Assay for Cytokines and Apoptosis-Related Molecules

We also performed RNA protection assay for control, NK911 (10 mg/kg), and doxorubicin (1.6 mg/kg) groups (n=12 each) at 1 week after the balloon injury in the injured carotid artery that was flash-frozen in liquid nitrogen. The stored artery was homogenized using the Isogen kit (WAKO), and mRNA was isolated. The mRNA expression was examined by RNA protection assay (RPA) using RNA template kit, RPA kit, and transcription kit (Farmingen, San Diego, Calif). The actual mRNA expression was corrected by GAPDH signal in each column.

Tissue Concentration of Doxorubicin

For measurement of tissue concentration of doxorubicin, the carotid arteries from the 3 groups were carefully excised and flashed by saline and weighed. The measurement was made at 8 time points, including before and 3 hours after the first drug administration on day 1, before and 3 hours after drug administration on day 3, on day 4, before and 3 hours after drug administration on day 6, and on day 7 (4 animals for each time point). In a single injury model, we also measured the concentration of doxorubicin in the contralateral artery. The measurement of doxorubicin was performed by the HPLC method.[21]

Possible Side Effects of NK911

We measured body weight on a weekly basis, whereas we measured hemodynamic variables (by the tail-cuff method in conscious conditions) and liver/renal functions at 4 weeks after balloon injury with NK911 administration. We also checked hematology at 1 and 4 weeks after the NK911 treatment.

Statistical Analysis

Statistical analysis was performed by unpaired Student's t test or ANOVA followed by Scheffé's post hoc test. A value of $P<0.05$ was considered to be statistically significant.

Results

Animal Assignment

We used a total of 398 rats. In the protocol on the time-course of vascular permeability, we used 18 rats (3 each for 6 time

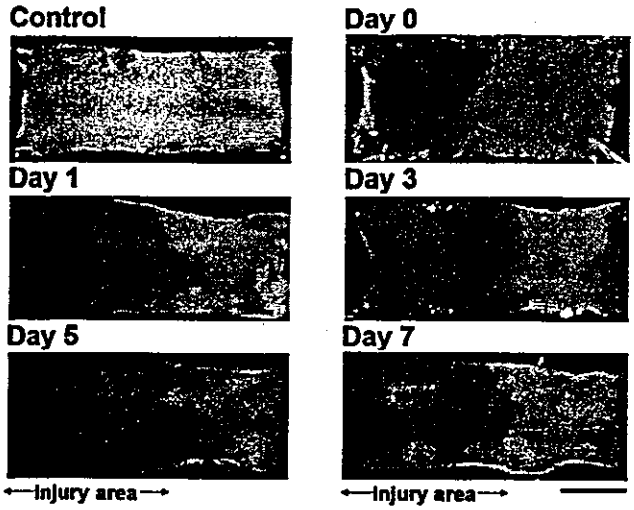

Figure 1. Sustained vascular hyperpermeability after balloon injury. Sustained hyperpermeability of the rat carotid arteries after balloon injury was demonstrated by Evans-Blue staining. Control specimen indicates noninjured carotid artery. In other specimens, the left side of the carotid artery (indicated by arrows) was the injured area for each time point. Bar=1 mm.

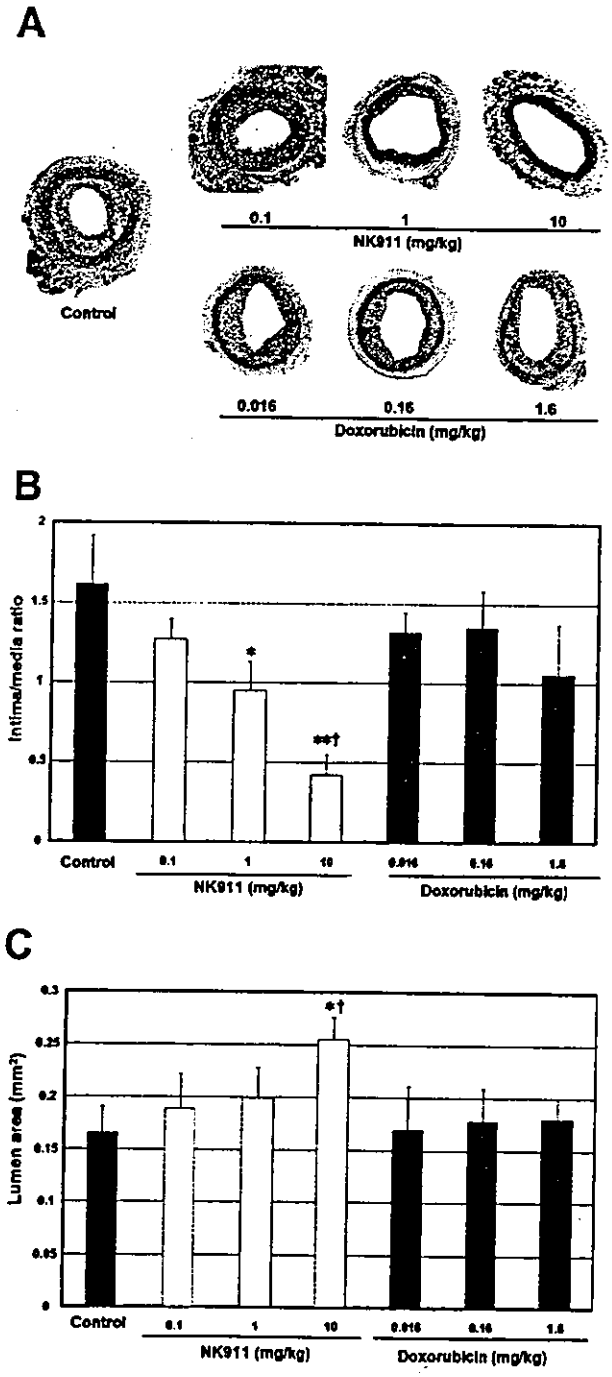

points after balloon injury). In the histology protocol, we used 48 in the single-injury model (3 different doses of NK911 and doxorubicin alone) and 36 in the double-injury model (2 different doses of NK911 and doxorubicin alone). For immunostaining protocol at 1 week after the injury, we used 48 for 3 different doses of NK911 and doxorubicin alone, while we used another 48 more for cell count protocol in the same manner. Finally, we used 128 for measurement of tissue concentration of doxorubicin (4 each at 8 time points after either a single or double balloon injury for NK911 and doxorubicin alone), while we used the remaining 72 for RPA analysis.

Sustained Increase in Vascular Permeability After Balloon Injury

We first examined the time-course of the increase in vascular permeability at 6 time points after balloon injury using Evans-Blue dye staining (n= 3 each). The balloon-injured area was blue-stained, and the staining was noted at least for 7 days after the injury, confirming the presence of the EPR effects in the balloon-injured artery (Figure 1).

Inhibitory Effect of NK911 in a Single-Injury Model

We then examined whether NK911 inhibits vascular lesion formation 4 weeks after a single balloon injury in the rat carotid artery. When compared with the control group (balloon injury with no treatment), NK911 significantly and dose-dependently inhibited neointimal formation as evaluated by intima/media ratio (Figures 2A and 2B) and therefore maintained the lumen area at a maximum dose, whereas doxorubicin alone showed no inhibitory effects and failed to prevent the reduction in lumen area (Figure 2C). The inhibitory effect of NK911 was noted at a dose of 1.0 mg/kg (0.16 mg/kg of doxorubicin), which is approximately one fourth of its effective concentration for the treatment of cancers.[22] In contrast, neither NK911 nor doxorubicin alone affected vascular remodeling (reduction in total cross-sectional area) as evaluated by the length ratio of IEL and EEL (data not shown).

Measurement of doxorubicin concentration in the balloon-injured artery showed that NK911 delivered the antiproliferative agent more effectively than intravenous administration of the drug alone to the balloon-injured arteries, whereas the concentration was low in the contralateral arteries at all time points (Figure 2D). Especially at 3 hours after the balloon injury, the doxorubicin

Figure 2. Inhibitory effects of NK911 in a single-injury model. A, Photomicrographs (H&E staining) of the balloon-injured rat carotid artery. Top, NK911 group. Bottom, Doxorubicin alone group. B and C, Intima/media ratio (B) and lumen area (C) of the balloon-injured rat carotid artery. Results are expressed as mean±SEM (n=6 each). *P<0.05, **P<0.01 vs control group; †P<0.05 vs doxorubicin-alone group at a corresponding concentration. D, Tissue doxorubicin (DOX) concentrations in the balloon-injured and the contralateral rat carotid arteries. Arrows indicate the injection timing of NK911 or doxorubicin. Results are expressed as mean±SEM. ***P<0.001 vs other groups; †P<0.05 vs doxorubicin-alone group at a corresponding concentration; §P<0.05 vs contralateral artery in the same animals.